Published in final edited form as:
Nat Commun. ; 3: 760. doi:10.1038/ncomms1759.

Poly(ADP-ribose) controls DE-cadherin-dependent stem cell maintenance and oocyte localization

Yingbiao Ji and **Alexei V. Tulin**
Epigenetics and Progenitor Cell Program, Fox Chase Cancer Center, Philadelphia, PA 19111

Abstract

Within the short span of the cell cycle, Poly(ADP-ribose) (pADPr) can be rapidly produced by Poly(ADP-ribose) Polymerases (PARPs) and degraded by Poly(ADP-ribose) Glycohydrolases (PARGs). Here we show that changes in association between pADPr and heterogeneous nuclear ribonucleoproteins (hnRNPs) regulate germline stem cell maintenance and egg chamber polarity during oogenesis in *Drosophila*. The association of pADPr and Hrp38, an ortholog of human hnRNPA1, disrupts the interaction of Hrp38 with the 5′UTR of DE-cadherin mRNA, thereby diminishing DE-cadherin translation in progenitor cells. Following the reduction of DE-cadherin level, germline stem cells leave the stem cell niche and differentiate. Defects in either pADPr catabolism or Hrp38 function cause a decreased translation of DE-cadherin, leading to a loss of germline stem cells and mislocalization of oocytes in the ovary. Taken together, our findings suggest that Hrp38 and its association with pADPr control germline stem cell self-renewal and oocyte localization by regulating DE-cadherin translation.

Keywords

poly(ADP-ribose); Hrp38; PARG; DE-cadherin; Oogenesis; stem cell; translation; IRES; tissue polarity; *Drosophila*

INTRODUCTION

In *Drosophila*, oogenesis begins with the asymmetrical division of one germline stem cell (GSC) into two: one GSC for self-renewal and one cystoblast that differentiates within the germarium (1). Maintenance of GSCs is controlled by several pathways (2–6), including the regulation of DE-cadherin expression that promotes anchoring of GSC to its niche through adherens junctions (6). Subsequently, one GSC daughter cell, the cystoblast, loses contact with the GSC niche and divides four times to form a cyst consisting of 15 nurse cells and an oocyte (7). Upon completion of proliferation, migration, and differentiation of follicle stem cells in the middle of the germarium, a monolayer of follicle cells surrounds this 16-cell cyst to form an egg chamber (8). During the last germarial stage, the elevated DE-cadherin-dependent adhesion between the oocyte and its surrounding follicle cells helps anchor the oocyte in the posterior pole, establishing the anterior-posterior axis of an egg chamber (9,10).

ADDRESS CORRESPONDENCE TO: Alexei V. Tulin, Ph.D., Fox Chase Cancer Center, 333 Cottman Avenue, Philadelphia, PA 19111, Tel: (215) 728-7408, Fax: (215) 728-2412, Alexei.Tulin@fccc.edu.

AUTHORS CONTRIBUTIONS: Y.J. and A.V.T. designed research; performed research; contributed new reagents/analytic tools; analyzed data; and wrote the paper.

COMPETING FINANCIAL INTERESTS: The authors declare no competing financial interests

Our present study demonstrates that Poly(ADP-ribose) (pADPr) association with heterogeneous nuclear ribonucleoproteins (hnRNPs) controls DE-cadherin expression. HnRNPs are ubiquitous RNA-binding proteins associated with pre-mRNA/mRNA in the nucleus and/or cytoplasm of the cell during transcription and post-transcriptional possesses (11–17). Poly(ADP-ribose), a polymer formed from 2 to 200 ADP-ribose units, is produced by Poly(ADP-ribose)polymerase-1 (PARP1) using NAD as a substrate (18). Non-covalent association of PARP1-pADPr with hnRNP decorates this protein with negative charges and prevents its binding to RNA (18). This regulation depends on the activity of PARP1, which adds pADPr to proteins (19), and PARG, which removes pADPr (20). Here we show that a high level of pADPr titrates Hrp38--an ortholog of human hnRNPA1--away from DE-cadherin mRNA and blocks Hrp38-dependent translation. Furthermore, we show that pADPr binding to Hrp38 is essential for germline stem cell function and oocyte positioning during oogenesis.

RESULTS

pADPr is enriched in *Drosophila* ovary

We determined the level of pADPr accumulation in different tissues of adult *Drosophila* by Western blotting. The largest amount of pADPr accumulated in the ovary, for which multiple bands of pADPr were observed (Figure 1a). To track *in vivo* pADPr accumulation in ovary, we cultured a dissected *Drosophila* ovary in the presence of biotinylated NAD ($_b$NAD). Previously, we reported that PARP1 converts $_b$NAD into $_b$pADPr (21). We examined 437 germaria and observed 31 dividing GSCs, all exhibiting the highest level of biotin labeling (Figure 1b–d). GSCs in the interphase did not incorporate any $_b$NAD (Figure 1c–d). We detected severe “punctate” labeling by $_b$NAD in cystoblasts (Figure 1c–d, arrows). High levels of biotin labeling persisted during maturation of germline cysts starting from region 1 of germarium (Figure 1c–e), yet labeling was depleted in the oocyte in stage 9 (Figure 1f). These findings imply the potential importance of pADPr turnover for progression of early oogenesis.

The *Parg* gene is required for oocyte localization

Since PARG removes pADPr to promote dynamic turnover of pADPr, we expected to find that PARG is required for normal oogenesis. Indeed, we detected *Parg* mRNAs in follicle and germline cells in wild-type ovaries using RNA *in situ* hybridization with an antisense *Parg* RNA probe (Figure 2a–b, Supplementary method S1). Ectopically expressed PARG-EGFP was localized to the nucleoplasm of nurse cells and the oocyte in stage 7 egg chambers, confirming that PARG recycles pADPr in nuclei of the ovary cells (Figure 2c). To test whether the *Parg* gene is essential for oogenesis, we generated *Parg* mutant clones in the ovary using the FRT/FLP system. Wild-type clones (Figure 2d), as well as egg chambers with *Parg* mutant germline clones (n=73) only or follicle cell clones only (n=91) did not show oocyte mislocalization (Figure 2e–f). However, egg chambers bearing *Parg* mutant clones, both in the follicle cells, including the polar cells, and the germline cells, exhibited mislocalization of the oocyte to its midpoint (36% (n=45), Figure 2g–h). These results show that loss of *Parg* in both germline and polar cell clones is a precondition for oocyte mislocalization in the *Parg* mutant.

The *hrp38* mutants have reduced fertility

To characterize the functions of the *hrp38* gene during *Drosophila* development, we used one P-element insertion in exon 2 of the *hrp38* gene (w^*,*P[XP]*$^{d05172/}$*TM6B, Tb*^{1}) (22) and a *hrp38* region deficiency line (w^{1118}; *Df(3R)*^{Exel6209}, *P{XP-U}*^{Exel6209}/*TM6B, Tb*^{1}) having a small deletion in exon 2 of the *hrp38* gene (23) (Supplementary Figure S1a). These mutations are lethal when homozygous. The *hrp38* hemizygotes (*hrp38*^{d05172}/*Df*) did not

express *hrp38* mRNA (Supplementary Figure S1b), and had a significantly lower expression of Hrp38 protein than the wild type at the third-instar larvae stage (Supplementary Figure S1c). In the complementation test, the P-element insertion ($hrp38^{d05172}$) failed to complement the *hrp38* deficiency (Supplementary Table S1). Two thirds of the *hrp38* hemizygotes ($hrp38^{d05172}/Df$) (n=682) died before the pupal stage, indicating the importance of *hrp38* for normal fly development. The incomplete penetrance may have proceeded from a partial overlap of *hrp38* and *hrp36*, whose functional domains are highly homologous (24).

We crossed *hrp38* RNAi lines (P{GD14939}v29523 and P{GD14939}v29524/CyO) with strains ubiquitously expressing GAL4 (*Act5C–GAL4* and *tubP–GAL4*). The results show that *hrp38* RNAi causes lethality (Supplementary Table S1). The expression of a *UAS-Hrp38:RFP* transgene induced by the ubiquitously expressed arm-*GAL4* driver was sufficient to rescue lethality of the hemizygotes ($hrp38^{d05172}/Df$) (Supplementary Figure S1d and Table S2). These results confirm that mutations of the *hrp38* gene are fully responsible for lethality of the hemizygotes ($hrp38^{d05172}/Df$). We observed that hemizygous female escapers had very low fertility (6 progeny/fly in the mutant versus 51 progeny/fly in the wild-type after 5 days of crossing; n=100) and significantly reduced egg laying rates (0.1 egg/hour/fly versus 1.2 egg/hour/fly respectively), confirming that the *hrp38* gene is required for oogenesis.

The *hrp38* gene regulates oocyte localization

Since the *hrp38* mutants have reduced fertility, we investigated *hrp38* functions during oogenesis. We observed that the Hrp38:GFP fusion protein in a protein trap line (ZCL588), in which GFP was spliced in the frame with the Hrp38-PE transcript (19), was predominantly expressed in nuclei of the somatic follicle cells and germline cells during all stages of oogenesis (Figure 3a–b). Since Hrp38:GFP expression is absent in the oocyte from stage 2 (Figure 3b), it appears that Hrp38 expression is inhibited in the oocyte once the cyst moves down the germarium after anterior-posterior axis is established. Therefore, we compared progression of oogenesis in the wild- type and *hrp38* mutant.

In a wild-type ovariole, all oocytes showing stronger Orb staining were positioned in the posterior pole adjacent to a pair of polar follicle cells stained with FasIII (Figure 3c). *hrp*38 mutant females displayed defects during egg development, including fused egg chambers (7%, (n=125), Figure 3d) and mislocalization of the oocyte (11%, (n=142), Figure 3e). Mispositioned oocytes in the *hrp38* mutants were found either at the anterior pole (Figure 3e, S6 egg) or on the lateral side of the egg chamber (Figure 3e, S5 egg). In the S5 egg, a pair of polar cells was separated from each other instead of the usual connection in the poles (Figure 3e, S5 egg), suggesting that Hrp38 is involved in defining the follicle cell patterns. The wild-type showed none of these defects (n=135) (Figure 3c). Expression of a *UASp-hrp38:RFP* transgene in the germline cells fully rescued the defective phenotypes of the *hrp38* hemizygotes ($hrp38^{d05172}/Df$) (n=216, Supplementary Figure S2a–b), confirming that *hrp38* loss-of-function mutation is responsible for the observed phenotypes. Although Hrp38 function is necessary for tissue polarity and oocyte positioning (Figure 3d–e), this protein was not required for asymmetric localization of cytoplasmic markers such as Gurken (Figure 3f–g). According to this last observation, Hrp38 controls tissue polarization by regulating extracellular interaction rather than polarization of cytoplasm within cells.

Parg and *Hrp38* control DE-cadherin-dependent oocyte localization

It is well known that the posterior localization of the oocyte requires cadherin-dependent adhesion between the follicle cells surrounding the posterior pole and the oocyte (9,10). As reported previously (9), DE-cadherin concentration in wild-type ovaries is considerably

greater at the interface between the oocyte and posterior follicle cells than between nurse cells and anterior follicle cells (Figure 4a). In *hrp38* mutant egg chambers, DE-cadherin expression was the highest at the anterior part of the egg chamber, a condition resulting in mislocalization of the oocyte to the anterior end (Figure 4b, green arrow). The *hrp38* mutant had lower expression of DE-cadherin at the adherens junctions (AJ) of the lateral follicle cells (Figure 4b, yellow arrow) relative to the wild-type (Figure 4a, yellow arrow). The altered expression of DE-cadherin was shown in 20% of *hrp38*−/− mutant egg chambers (n=130), among which 75% had relatively higher expression in the anterior than in the posterior pole, while 25% had no accumulation. All these egg chambers displayed either oocyte mislocalization or fused egg chambers. Immunoblotting analysis showed that DE-cadherin expression in the *hrp38* mutant ovary was approximately 3-fold decreased relative to the wild-type ovary (Supplementary Figure S3a). Germline expression of the *UASp-hrp38:RFP* transgene restored the normal expression pattern of DE-cadherin in the *hrp38* mutant egg chambers (n=90; Supplementary Figure S2c), confirming that *hrp38* loss-of-function causes decreased DE-cadherin expression in the ovary.

To test whether reduced expression of DE-cadherin is responsible for oocyte mislocalization in the *hrp38* mutants, we cloned the *DE-cadherin* coding region without its 5′ UTR into *pUASp* vector and used nos-GAL4 to drive expression of the transgene in germline cells in the *hrp38* mutant background (Figure S3a). DE-cadherin expression in the germline cells was sufficient to restore normal oocyte localization in the *hrp38* mutants (n=112) (Supplementary Figure S3b–c). After expressing DE-cadherin transgene in the germline cells, we did not observe any phenotypes exhibited by the *hrp38* mutant (n=136, Supplementary Figure S3d–e). This finding shows that proper oocyte polarity established by DE-cadherin-mediated adherens junctions in the germarium also affects the fate of stalk and polar follicle cells in the later stages of oogenesis. Taken together, these results suggest that decreased DE-cadherin expression in the germline cells is the underlying cause for the observed phenotypes in the *hrp38* mutant.

Consistent with oocyte mislocalization observed in *Parg* mutant follicle and germline cell clones (Figure 2g–h), the loss of *Parg* in both germ cells and polar cells led to loss of DE-cadherin expression (compare Figure 4c–e). Expression of a *pUASp-DE-cadherin* transgene without its 5′UTR in the germline cell using nos-Gal4 driver was sufficient to rescue the oocyte mislocalization in the *Parg* mutant follicle, including the polar cells and germline cell clones (n=34, Figure 4g–h). Therefore, loss of DE-cadherin expression is responsible for oocyte mislocalization in *Parg* mutant clones.

These results show that the *hrp38* and *Parg* genes regulate the expression of DE-cadherin, required for proper oocyte positioning. Since Hrp38 shows greater association with pADPr in the *Parg* mutant than in the wild type (19), we proposed that pADPr binding to Hrp38 regulates DE-cadherin expression. To test this hypothesis, we removed one copy of the *Parg* gene in the *hrp38* mutant background (*Parg*−/+; hrp^{d05172}/Df). The mutant genotype (*Parg*−/+;hrp^{d05172}/Df) had an increased proportion of mislocalized oocytes relative to the *hrp38* mutant alone (19% vs. 11% respectively, n=176; *t*-test P <0.05). Most of the mislocalized oocytes in the genotype (*Parg*−/+;hrp^{d05172}/Df) showed no accumulation of DE-cadherin in either pole, resulting in laterally positioned oocytes (Figure 4f, arrow), which resembled the phenotypes caused by DE-cadherin null mutation (10). Expression of *Hrp38:RFP* (n=152) or *DE-cadherin* transgene (n=165) in the germline fully rescued oocyte mislocalization in (*Parg*−/+; hrp^{d05172}/Df).

Hrp38 controls germline stem cell maintenance

Besides oocyte localization, DE-cadherin is required for germline stem cell maintenance by anchoring GSCs within the niche through adherens junctions (6) (Figure 5a). If controlling

DE-cadherin levels is a general function of pADPr binding to Hrp38, *hrp38* and *Parg* mutants should display defects in DE-cadherin-mediated regulation of GSCs. Indeed, we found that Hrp38:GFP is expressed in GSCs, as well as in cap cells of the GSC niche (Figure 5b). Similar to the wild-type (n=85), most germaria of *hrp38* mutants had two or three GSCs at day 3 after eclosion (n=82) (Supplementary Figure S4a). At day 10, wild-type germaria had two or three GSCs (n=94) (Figure 5c), while most germaria in the *hrp38* mutant (72%) had only one GSC left (n=91) (Figures 5d and Supplementary Figure S4a). Seventeen days after eclosion, 70% of germaria in the *hrp38* mutants had lost their GSCs (n=96) (Figures 5e–f and Supplementary Figure S4a), while the wild-type still retained GSC self-renewal ability (n=90) (Figure 5f). The expression of the *hrp38:RFP* transgene in the germline cells restored GSC self-renewal ability of the *hrp38* mutant (Figure 5f, Supplementary Figure S4a and S4b), confirming that the *hrp38* gene is required for GSC maintenance.

DE-cadherin is strongly expressed in the interface between GSCs and cap cells in the wild-type fly (6) for anchoring the GSC within the niche (Figure 5g). We examined DE-cadherin expression in 10-day-old wild-type and *hrp38* mutant GSCs (Figure 5g–h). DE-cadherin expression level at the interface between the cap cells and the one remaining GSC in 10-day-old *hrp38* mutants was reduced by 70%, relative to that in the wild-type (n=10, Figure 5h). Normal expression levels of DE-cadherin in the interface between cap cells and GSC were restored by expressing *UASp-hrp38:RFP* transgene in GSCs in 14-day-old *hrp38* mutants (n=128, Supplementary Figure S4c). Ectopic expression of DE-cadherin in the germline significantly increased the GSC self-renewal ability in the *hrp38* mutant background (Figures 5f, Supplementary Figure S4d–f), confirming that decreased DE-cadherin expression causes the loss of GSC self-renewal ability in the *hrp38* mutants.

To maintain their undifferentiated state, GSCs must keep low levels of Bag-of-marbles (BAM) differentiation factor (25–27). Compared to the wild-type fly (n=54, Supplementary Figure S5a), BAM was not prematurely expressed in the *hrp38* mutant GSCs (n=58, Supplementary Figure S5b). Using anti-cleaved Caspase-3 antibody, which has been used successfully to detect apoptosis in the *Drosophila Lsd1* mutant GSC (28), we did not detect strong apoptosis signals in the GSC of 10-day-old *hrp38* mutants (n=58, Supplementary Figure S5b). These observations largely exclude the possibility that either premature differentiation of GSC through the BAM-dependent pathway or apoptosis caused the loss of GSC maintenance in the *hrp38* mutant.

Parg and *Hrp38* control DE-cadherin–dependent stem cell maintenance

Because *Parg* mutant germline cell and follicle cell clones lost the expression of DE-cadherin (Figure 4d), we investigated whether *Parg* is required for GSC self-renewal. We found that *Parg* mRNA and PARG-EGFP are expressed in the wild-type GSCs (Figure 6a and Supplementary Figure S5c) and by germline-specific GAL4 driver (Figure 6b). To determine whether *Parg* is required for GSC self-renewal, we used a FLP/FRT recombination system to generate negatively labeled *Parg* mutant GSCs, which were identified by the absence of GFP expression (Figure 6c–d). The loss rates of the mutant GSCs were computed based on a published procedure (6). Three days after clone induction, *Parg* mutant GSCs and cysts were present in the germarium (n=53) (Figure 6c). Two weeks after clone induction, *Parg* mutant GSCs were lost in 95% of the germaria (n=58, Supplementary Figure S5d) where the developing *Parg* mutant egg chamber was visible (Figure 6d). Marked wild-type GSCs were still retained in 80% of germaria (n=56, Supplementary Figure S5d). Therefore, we conclude that *Parg* is required for maintaining GSCs and infer that poly(ADP-ribosyl)ation strongly affects GSC maintenance.

To test whether the *hrp38* and *Parg* genes interact to control GSC maintenance, we assessed the changes in number of GSCs in (*Parg*−/+;*hrp*^{d05172}/*Df*) genotype with aging. Removing one copy of the *Parg* gene caused a more rapid GSC loss in the *hrp38* mutant (Figures 5f and Supplementary Figure S4a). Expression of *Hrp38:RFP* or *DE-cadherin* transgenes in the germline fully restored GSC maintenance ability (*Parg*−/+;*hrp*^{d05172}/*Df*) (Supplementary Figure S4a). These results demonstrate that genetic interaction between the *hrp38* and *Parg* genes controls GSC maintenance.

Further, we examined DE-cadherin expression in *Parg* mutant GSC clones one week after clone induction. DE-cadherin accumulated in the interface between the wild-type GSC (GFP-positive) and wild-type cap cells, yet its expression was 4-fold reduced in *Parg* mutant GSC clones (GFP-negative) when compared to DE-cadherin accumulation in wild-type GSC cells (Figure 6e–f) (n=10). With expression of the *DE-cadherin* transgene in the germline cells (Figure 6g–h), the *Parg* mutant GSCs were still maintained in 65% of germaria (n=70) two weeks after clone induction, which is comparable to the maintenance rate of the marked wild-type GSCs (Supplementary Figure S5d). Therefore, the loss of DE-cadherin expression, resulting in the failure to strongly anchor the *Parg* mutant GSC within the niche by adherens junctions, likely explains the *Parg* mutant's loss of GSC self-renewal. Similar to *hrp38* mutant GSCs, *Parg* mutant GSCs were lost neither by apoptosis (Supplementary Figure S5e–f) nor by inappropriate expression of Bam (Supplementary Figure S5g–h).

pADPr inhibits Hrp38-dependent DE-cadherin translation

To further evaluate how pADPr binding to Hrp38 controls DE-cadherin expression, we examined mRNA and protein expression levels of DE-cadherin in the *hrp38* and *Parg* mutants at the third-instar larval stage. We found no significant difference in mRNA expression levels between the wild-type and the *hrp38* mutant or the *Parg* mutant by qRT-PCR (Supplementary method S2) (Figure 7a), suggesting that pADPr binding to Hrp38 doesn't affect DE-cadherin transcription. Although the *DE-cadherin* gene has only one transcript with a constitutively spliced intron (Flybase), we examined potential effects of *hrp38* or *Parg* mutation on splicing of *DE-cadherin* transcript. Splicing defects were not observed in *hrp38* and *Parg* mutants, suggesting that Hrp38 and its association with pADPr don't regulate DE-cadherin by affecting splicing. Immunoblotting analysis (Supplementary method S2) showed that protein expression levels of DE-cadherin in *hrp38* and *Parg* mutants was decreased by 3.5- and 4.0-fold respectively, relative to the wild-type (Figure 7b), suggesting that the association of Hrp38 with pADPr regulates DE-cadherin expression at the translational level.

Next, we tested whether Hrp38 protein could bind to DE-cadherin mRNA directly in the ovary. Using UV-crosslinking, biotin-labeled probes were made from three distinct regions (5′UTR, coding region, and 3′UTR) of DE-cadherin (Figure 7c). UV-crosslinking experiments showed that Hrp38 binds only to the 5′UTR of DE-cadherin mRNA in wild-type ovaries (Figure 7d). Association of Hrp38 with *DE-cadherin* transcripts was further verified by *in vivo* RNA immunoprecipitation (IP) (Supplementary method S3) using anti-Hrp38 antibody in *Drosophila* ovary (Supplementary Figure S6a–b).

Our previous study demonstrated that pADPr binding to Hrp38 reduced ability of this protein to bind RNA (19). In humans, pADPr modification is known to inhibit the RNA-binding ability of hnRNP A1 (19), the mammalian homolog of Hrp38 (29). To assess the role of Hrp38 modification by pADPr in *Drosophia*, we tested whether poly(ADP-ribosyl)ation could inhibit Hrp38 binding to the 5′UTR of DE-cadherin using UV-crosslinking. Total protein was extracted from wild-type or *Parg* mutant third-instar larvae and was cross-linked to the 5′UTR of DE-cadherin. The amount of Hrp38 protein binding to the 5′UTR of DE-cadherin was 3.8-fold decreased in the *Parg* mutant, relative to that in the

wild-type, suggesting that association with pADPr inhibits Hrp38 binding to the 5′UTR of DE-cadherin (Figure 7e).

Based on the finding that human hnRNP A1 has the strongest binding affinity to the G-rich RNA element (UAUGAUAGGGACUUAGGGUG) (30), a potential binding site of Hrp38 (413-CAGGGCGCGCACUGUACGAG-432 bp) was identified within the DE-cadherin 5′UTR region. To test if Hrp38 could bind to this G-rich motif, Hrp38 proteins were generated and purified (Supplementary Figure S6c). The dot-blot assay confirmed that pADPr binds to Hrp38 protein *in vitro* (Figure S6d). An electrophoretic mobility shift assay showed that Hrp38 binds to this RNA motif (Figure 7f, lane 3). Preincubation of Hrp38 protein with pADPr almost completely abolished Hrp38 binding to this RNA motif (Figure 7f, lane 4). This result confirms that pADPr strongly inhibits the interaction between Hrp38 and RNA *in vitro* and provides additional evidence that association with pADPr inhibits Hrp38 binding to the 5′UTR of DE-cadherin.

Hrp38 is required for IRES-dependent *DE-cadherin* translation

The 5′UTR (686 bp) of *DE-cadherin* is much longer than the average size of 256 bp in 5′ UTR of *Drosophila* genes (31), implying that the *DE-cadherin* 53UTR may have the ability to initiate an Internal Ribosome Entry Site (IRES)-mediated translation. Nucleotide sequence of IRES allows translation initiation in the middle of an mRNA sequence (32). To test whether Hrp38 binding to the DE-cadherin 5′UTR promotes IRES-dependent translation, the 5′UTR of *DE-cadherin* was cloned into the upstream sequence of the firefly luciferase gene in Renilla/Firefly luciferase reporter plasmid (Figure 7g). After transfection into *Drosophila* S2 cells, firefly and renilla luciferase activities were measured. As a positive control, the Polio virus IRES showed ten-fold increase of luciferase activity relative to the control construct (pNo-IRES) (Figure 7h). In contrast, the luciferase activity in cells transfected with DE-cadherin 53UTR construct (p5′UTR-DEcad) was increased 40-fold, relative to the control construct (Figure 7h). The efficient induction of IRES-mediated translation by the DE-cadherin 5′UTR is similar to that found in the 5′UTRs of other genes in *Drosophila* (33). Neither the DE-cadherin 53UTR in reverse orientation, as a spacer control, nor DE-cadherin 33UTR, as an element control, show a significant increase in firefly luciferase activity, relative to the control (Figure 7h). Consequently, the DE-cadherin 53UTR has a strong ability to induce IRES-mediated translation. Furthermore, *in vivo* RNA immunoprecipitation (IP) showed that Hrp38 was associated with the transcript from *DE-cadherin*-5′UTR luciferase construct after transfection into *Drosophila* S2 cells (Figure 7i–j), suggesting that Hrp38 is an IRES transacting factor for promoting cap-independent translation of *DE-cadherin* mRNA.

DISCUSSION

Our experimental findings suggest that pADPr binding to *Drosophila* hnRNP A1 homolog Hrp38 regulats stem cell maintenance and oocyte polarity. Earlier research demonstrated that Hrp38 regulates alternative splicing (AS) (19, 34), while hnRNP A1 was reported to control translation initiation through an IRES-mediated mechanism by binding to the 5′UTR of regulated genes (35, 36). Here we show that pADPr association with Hrp38 controls DE-cadherin translation through an IRES–mediated mechanism. Since Hrp38 binds to the 5′UTR of DE-cadherin and is associated with the *DE-cadherin* 5′UTR-luciferase transcript, it seems very likely that Hrp38 is an IRES transacting factor for promoting DE-cadherin translation. In mammals, post-translational modification of hnRNP A1 has been shown to regulate IRES-dependent translation. For instance, phosphorylation of hnRNP A1 can promote the binding of hnRNP A1 to IRES of c-*Myc* in myeloma cells (37). Similarly, our results suggest that pADPr modification of hnRNPs negatively regulats IRES-mediated translation by inhibiting the binding of hnRNPs to IRES.

The inhibitory function of pADPr binding to hnRNPs likely occurs in the nucleus for two reasons. First, Hrp38 is predominantly a nuclear protein that binds to the 5′UTR of DE-cadherin presumably in the nucleus. Second, pADPr metabolism is mainly localized in the nucleus. This inference is consistent with a currently accepted model suggesting that IRES transacting factors, such as hnRNP A1, are associated with IRES-containing mRNA in the nucleus from the beginning (38). However, since recent research has shown that pADPr can regulate microRNA-mediated translation in the cytoplasm (39), it is entirely plausible that poly(ADP-ribosy)lation also functions in the cytoplasm to inhibit IRES-mediated translation.

Our finding that pADPr modification of Hrp38 regulates DE-cadherin expression in the ovary reveals how DE-cadherin expression is regulated during oocyte localization. The localization of the oocyte in the posterior end occurs during the transition from region 2b to region 3 in the germarium (10). We found that Hrp38 is also expressed in the oocyte and its surrounding follicle cells in region 2b of the germarium (Figure 3a). We also found that the *hrp38* mutant has a lower expression of *DE-cadherin* at the interface between the oocyte and surrounding posterior cells, implying that the *hrp38* gene is required for upregulating DE-cadherin expression for oocyte localization. Therefore, we suggest that Hrp38 is required for upregulation of DE-cadherin expression in both the oocyte and surrounding follicle cells by promoting translation (Figure 8c). Basically, the expression of Hrp38 in the oocyte and surrounding follicle cells in region 2b helps increase the translation of DE-cadherin by binding to the 5′ UTR of *DE-cadherin* mRNA. The newly produced DE-cadherin assists with anchoring the oocyte in the posterior pole. In mid-body follicle cells and nurse cells, Hrp38 association with pADPr can downregulate DE-cadherin expression (Figure 4e). Since expression of the DE-cadherin transgene in the germline was sufficient to rescue oocyte mislocalization in the *Parg* mutant double clones (Figure 4h), our finding supports the notion that *DE-Cadherin* germline mutant clones alone aren't sufficient to cause oocyte mislocalization (40, 41). In summary, we have identified a novel pathway that regulates stem cell maintenance and oocyte polarity via pADPr modification of an hnRNP protein (Hrp38) in *Drosophila* (see Supplementary Discussion for broader implications of these findings).

METHODS

Drosophila strains and genetics

Flies were cultured on standard cornmeal-molasses-agar media at 25°C, unless otherwise indicated. The following stocks were from Bloomington Stock Centre: *arm:GAL4/Cyo* (#1560); *Act5C–GAL4/Cyo* (#4414); *tubP–GAL4/TM3* (#5538); *P{PTT-GC}Hrb98DE*^{ZCL0588} (Hrp38:GFP trap line, #6822); *y*^{1}, *w**, *v*^{24}, *P{FRT(w*^{hs}*)}101* (#1844). A P-element insertion of the *hrp38* gene (*w*,P[XP]*^{d05172}*/TM6B, Tb*^{1}*)* and a *hrp38* region deficiency line (*w*^{1118}*; Df(3R)Exel6209, P{XP-U}Exel6209/TM6B, Tb*^{1}) from the Exelixis Collection at the Harvard Medical School were replaced with the GFP-bearing balancer (*TM3, P{ActGFP}JMR2, Ser*^{1}) for selecting homozygous mutants. Two *Hrp38* RNAi lines (*w*^{1118}*; P{GD14939}v29523* and *w*^{1118}*; P{GD14939}v29524/CyO*) were from the Vienna Drosophila RNAi Centre. The *Parg* mutant (*Parg* $^{27.1}$*/FM7, Actin-GFP*) was described previously (42). The germline-specific GAL4 driver {*nos-Gal4*:VP16} was from Dr. Spradling's lab. The BAM-GFP reporter line was a gift from Dr. McKearin (27). The full-length Hrp38 PCR fragment amplified from a *hrp38* cDNA clone (LD383464) was cloned into pUAST-RFP(C-terminus fusion) and pUASp-RFP (C-terminus fusion) vectors through the *Drosophila* Gateway Vector Cloning System (Carnegie Institution of Washington). The full-length *DE-cadherin* coding region without its 5′UTR was amplified from DE-cadherin cDNA clone (RE37915) (DGRC) and cloned into pUASp vector (DGRC). The pUSAp-PARG:EGFP transgene was constructed by cloning the fused fragment of PARG cDNA

with EGFP into pUASp vector. All transgenic flies were obtained with the standard P-element-mediated transformation method.

Clonal analysis using the FRT-FLP system

The *Parg* female heterozygotes *(Parg$^{27.1}$/FM7a,w^{a})* were crossed with *y^{1}, w*, v^{24}, P{FRT(w^{hs})}101/Y* (43) to generate the FRT-bearing *Parg* mutation (*Parg$^{27.1}$, P{FRT(w^{hs})}101/FM7a,w^{a}*) by genetic recombination. To induce the follicle cell clones in the ovary, *Parg $^{27.1}$, P{FRT(w^{hs})}101/FM7a,w^{a}* was crossed with *w*, Ubi-GFP,P{FRT(w^{hs})}101/Y; P{en2.4-GAL4}e16E, P{UAS-FLP1.D}JD1/Cyo* (44). To induce the *Parg* mutant germline clones in the ovary, the newly enclosed adults (*Parg$^{27.1}$, P{FRT(w^{hs})}101/w*, Ubi-GFP,P{FRT(w^{hs})}101; P{hs::FLP}38/+*) from the progeny of *Parg$^{27.1}$, P{FRT(w^{hs})}101/FM7a* crossed with *w*, Ubi-GFP,P{FRT(w^{hs})}101/Y; P{hsFLP}38* (a gift from Dr. O'Reilly) were treated by heat-shock at 37°C every two hours during the daytime for two days. The *Parg* GSC (GSC) clones were identified based on the absence of GFP expression and the presence of the round fusome labeled by anti-*hts* antibody. The wild-type clones were generated using the line (*y^{1}, w*, v^{24}, P{FRT(w^{hs})}*101) using the same method. The loss rates of the mutant GSCs were counted at 3, 10 and 17 days after clone induction, respectively, based on the published procedure (6).

Biotinylated NAD assay to detect PARP1 activity

To detect PARP1 activity *in vivo*, we used an assay based on incorporation of biotin label donated from biotinylated NAD ($_{b}$NAD) to pADPr-proteins (21,45). Biotin incorporation detected after exposure to $_{b}$NAD is greatly enhanced over intrinsic cytosolic biotin signal. In *Drosophila*, the utilization of NAD is, in general, PARP1-dependent (21). To deliver $_{b}$NAD to tissues for the assay, we dissected *Drosophila* ovary, leaving exposed tissues in the presence of 2.5 nM $_{b}$NAD for 1 hour. Our previous experiments (21) demonstrate that a period of 30 – 60 minutes is sufficient for the detection of PARP1-dependent $_{b}$NAD utilization. After fixation with 4% paraformaldehyde, we detected the biotin label using Avidin-Rhodamine (Sigma), and visualized biotinylated pADPr by confocal microscopy.

Immunohistochemistry

Ovaries dissected in Grace's insect medium were fixed in 4% paraformaldehyde + 0.1% Triton X-100 in PBS for 20 min and blocked with 0.1% Triton X-100 + 1% BSA for two hours. These ovaries were then incubated with the primary antibody overnight at 4°C, washed 3 times with PBS + 0.1% Triton X-100, and incubated with fluorescence-labeled secondary antibody for two hours at room temperature. After washing three times with PBS + 0.1% Triton X-100, the filamentous actin in the cell membrane was stained with Alexa Fluor 568/633 phalloidin (1:40; Invitrogen) for 30 minutes, and/or the DNA nuclei were stained with DRAQ5 dye (1:500; Biostatus) for 10 minutes. The following primary antibodies were used: mouse anti-Orb (4H8, 1:20; DSHB), mouse anti-FasIII (7G10, 1:10; DSHB), mouse anti-Gurken (1D12, 1:10; DSHB), rat anti-DE-cadherin (DCAD2, 1:5; DSHB), rabbit anti-Vasa (1:200; Santa Cruz Biotechnology), mouse anti-hts (1B1,1:20; DSHB), mouse anti-Lamin C (LC28.26, 1:50; DSHB); mouse anti-BAM (1:10; DSHB); rabbit anti-RFP (1:1000, Clontech). Alexa Fluor 488/568 goat anti-mouse IgG1/Ig2a (1:400; Invitrogen) was used to detect anti-Orb (4H8, IgG1) and anti-FasIII (IgG2a) primary antibodies for double immunostaining. Alexa Fluor 488 goat anti-mouse, Alexa Fluor 568 anti-rabbit, and Alexa Fluor 633 anti-rat IgG(H+L) were used to detect other primary antibodies (1:400; Invitrogen). MetaMorph image analysis software (Molecular Devices) was used to quantify the confocal images when required.

RNA–protein UV-crosslinking analysis

Biotin-labeled RNA probes were made using 0.2 ug PCR templates amplified from DE-cadherin cDNA clone (RE37915) (DGRC) with DIG RNA labeling Kit (Roche). A UV-crosslinking assay was performed following published methods (46,47) with modifications for biotin-labeled probes. The protein lysate from ovaries or the third-instar larvae of the appropriate genotypes was extracted using polysome lysis buffer (100 mM KCl, 5 mM $MgCl_2$, 10 mM HEPES, pH 7.0, 0.5% NP-40, 1 mM DTT). The 50 ug lysate was incubated with 40 pg biotin-labeled RNA probe in a 50 ul volume with 5X binding buffer (50 mM Tris–HCl, 250 mM KCl, 5 mM DTT, pH 7.5) on ice for 15 minutes. The binding reaction was irradiated with 254 nm UV light for 10 minutes on ice using Spectrolinker UV Crosslinker (Krackeler Scientific, Inc., Albany, NY). The RNA probes were further digested with 10 ug RNAse A (Sigma) and 1000 unit RNAse T1 (Ambion) for 15 minutes at 37°C. For immunoprecipitation, the reaction with 150 ul polysome lysis buffer was incubated with the rabbit anti-Hrp38 antibody (34) or rabbit IgG (Sigma) (the negative control) at 1:20 dilution overnight and then with 30 μl protein A agarose (Invitrogen) for 2h at 4°C. The IP complex was washed using the lysis buffer three times and resolved in 4–12% PAGE gel (Invitrogen). The protein covalently linked to a stub of the biotin-labeled RNA probe was detected with stabilized streptavidin-horseradish peroxidase conjugate with chemiluminescent substrate (Pierce). The blot was stripped and probed with the rabbit anti-Hrp38 antibody (1:10000). All cross-linking experiments were repeated three times.

RNA Electrophoretic Mobility Shift Assay (EMSA)

RNA EMSA was performed as described earlier (19). The full-length Hrp38 protein was generated through the cleavage of GST tag by PreScission Protease (GE) from GST-Hrp38 recombinant protein, which was expressed from the GST-Hrp38 fusion protein plasmid (34) (a gift from Drs. Borah and Steitz). Hrp38 protein was further purified using GSTrap™ HP columns (GE Healthcare). Either 50 ng GST (BioVision) or 50 ng Hrp38 was incubated with 0.1 um biotin-labeled G-rich element (413-CAGGGCGCGCACUGUACGAG-432) within the 5′UTR of the *DE-cadherin* gene (IDT) in binding buffer (Pierce). For the pADPr inhibition assay, 50 ng Hrp38 was preincubated with 140 ng pADPr (Biomol) in 1X binding buffer for 20 min at 25°C. The experiment was repeated three times. The biotin signals from EMSA were detected with a chemiluminescent kit (Pierce) and measured using the Image J software (NIH).

Dual-luciferase Reporter Assay

A bicistronic luciferase reporter plasmid (pMB255) containing Polio virus IRES element (48) (a gift from Dr. Roegiers) was digested with *Kpn*I and *Eco*RV to remove Polio virus IRES completely. DE-cadherin 5′UTR and 3′UTR PCR products were cloned into the derived luciferase reporter in the forward or reverse orientation. The reporter plasmid (pMB255) was also digested with *Eco*RV and *Pml*I and religated as a negative control for firefly luciferase assay. *Drosophila* S2 cells were maintained at 22°C in the culture medium supplemented with 10% FBS and 1% penicillin/streptomycin. 0.5 X 10^6 cells per well were seeded into a 6-well plate and incubated for 24 hours before the transfection. 1ug plasmid of the different constructs was transfected into S2 cells using Effectene transfection reagent (Qiagen). After the incubation for 24 hours, the firefly and renilla luciferase activities were measured in triplicate using Dual-Luciferase® reporter assay system (Promega). The ratio of the firefly-to-renilla luciferase activity was calculated based on experiments performed in triplicate, beginning from the transfection. The statistical analysis was done based on Student's *t*-test.

Supplementary Material

Refer to Web version on PubMed Central for supplementary material.

Acknowledgments

We thank Drs. S. Borah, A. O'Reilly, F. Roegiers, H. Saumweber, J. A. Steitz and M. Takeichi for providing materials. Drs. Alana O'Reilly, Ekaterina Pechenkina and David Martin contributed valuable comments on the manuscript. This project is funded by the National Institutes of Health (R01 GM077452) to A.V.T.

References

1. Fuller MT, Spradling AC. Male and Female Drosophila Germline Stem Cells: Two Versions of Immortality. Science. 2007; 316:402–404. [PubMed: 17446390]
2. Xie T, Spradling AC. decapentaplegic Is Essential for the Maintenance and Division of Germline Stem Cells in the Drosophila Ovary. Cell. 1998; 94:251–260. [PubMed: 9695953]
3. Wang Z, Lin H. Nanos Maintains Germline Stem Cell Self-Renewal by Preventing Differentiation. Science. 2004; 303:2016–2019. [PubMed: 14976263]
4. Szakmary A, Cox DN, Wang Z, Lin H. Regulatory relationship among piwi, pumilio, and bag-of-marbles in Drosophila germline stem cell self-renewal and differentiation. Curr Biol. 2005; 15:171–178. [PubMed: 15668175]
5. Maines JZ, Park JK, Williams M, McKearin DM. Stonewalling Drosophila stem cell differentiation by epigenetic controls. Development. 2007; 134:1471–1479. [PubMed: 17344229]
6. Song X, Zhu CH, Doan C, Xie T. Germline Stem Cells Anchored by Adherens Junctions in the Drosophila Ovary Niches. Science. 2002; 296:1855–1857. [PubMed: 12052957]
7. de Cuevas M, Lilly MA, Spradling AC. Germline cyst formation in *Drosophila*. Annu Rev Genet. 1997; 31:405–428. [PubMed: 9442902]
8. O'Reilly AM, Lee HH, Simon MA. Integrins control the positioning and proliferation of follicle stem cells in the Drosophila ovary. J Cell Biol. 2008; 182:801–815. [PubMed: 18725542]
9. Godt D, Tepass U. Drosophila oocyte localization is mediated by differential cadherin-based adhesion. Nature. 1998; 395:387–391. [PubMed: 9759729]
10. Gonzalez-Reyes A, St Johnston D. The Drosophila AP axis is polarised by the cadherin-mediated positioning of the oocyte. Development. 1998; 125:3635–3644. [PubMed: 9716529]
11. Dreyfuss G, Kim VN, Kataoka N. Messenger-RNA-binding proteins and the messages they carry. Nat Rev Mol Cell Biol. 2002; 3:195–205. [PubMed: 11994740]
12. Norvell A, Kelley RL, Wehr K, Schüpbach T. Specific isoforms of Squid, a Drosophila hnRNP, perform distinct roles in Gurken localization during oogenesis. Genes & Development. 1999; 13:864–876. [PubMed: 10197986]
13. Hachet O, Ephrussi A. Drosophila Y14 shuttles to the posterior of the oocyte is required for oskar mRNA transport. Curr Biol. 2001; 11:1666–1674. [PubMed: 11696323]
14. Cáceres L, Nilson LA. Translational repression of gurken mRNA in the Drosophila oocyte requires the hnRNP Squid in the nurse cells. Developmental Biology. 2009; 326:327–334. [PubMed: 19100729]
15. Huynh JR, Munro TP, Smith-Litiere K, Lepesant JA, St Johnston D. The Drosophila hnRNPA/B Homolog, Hrp48, Is Specifically Required for a Distinct Step in osk mRNA Localization. Developmental Cell. 2004; 6:625–635. [PubMed: 15130488]
16. Yano T, et al. Hrp48, a Drosophila hnRNPA/B Homolog, Binds and Regulates Translation of oskar mRNA. Developmental Cell. 2004; 6:637–648. [PubMed: 15130489]
17. Jain RA, Gavis ER. The Drosophila hnRNP M homolog Rumpelstiltskin regulates nanos mRNA localization. Development. 2008; 135:973–982. [PubMed: 18234721]
18. Tulin A, Chinenov Y, Spradling A. Regulation of chromatin structure and gene activity by Poly(ADP-ribose) polymerases. Curr Top Devel Biol. 2003; 56:55–83. [PubMed: 14584726]
19. Ji Y, Tulin AV. Poly(ADP-ribosyl)ation of heterogeneous nuclear ribonucleoproteins modulates splicing. Nucl Acids Res. 2009; 37:3501–3513. [PubMed: 19346337]

20. Bonicalzi ME, Haince JF, Droit A, Poirier GG. Regulation of poly(ADP-ribose) metabolism by poly(ADP-ribose) glycohydrolase: where and when? Cell Mol Life Sci. 2005; 62:739–750. [PubMed: 15868399]
21. Tulin A, Spradling AC. Chromatin loosening by poly(ADP)-ribose polymerase (PARP) at Drosophila puff loci. Science. 2003; 299:560–562. [PubMed: 12543974]
22. Thibault ST, et al. A complementary transposon tool kit for Drosophila melanogaster using P and piggyBac. Nature Genetics. 2004; 36:283–287. [PubMed: 14981521]
23. Parks AL, et al. Systematic generation of high-resolution deletion coverage of the Drosophila melanogaster genome. Nature Genetics. 2004; 36:288–292. [PubMed: 14981519]
24. Haynes SR, Johnson D, Raychaudhuri G, Beyer AL. The Drosophila Hrb87F gene encodes a new member of the A and B hnRNP protein group. Nucleic Acids Research. 1991; 19:25–31. [PubMed: 1849257]
25. McKearin D, Ohlstein B. A role for the Drosophila bag-of-marbles protein in the differentiation of cystoblasts from germline stem cells. Development. 1995; 121:2937–2947. [PubMed: 7555720]
26. Chen D, McKearin D. Dpp signaling silences bam transcription directly to establish asymmetric divisions of germline stem cells. Current Biol. 2003; 13:1786–1791.
27. Li Y, Minor NT, Park JK, McKearin DM, Maines JZ. Bam and Bgcn antagonize Nanos-dependent germ-line stem cell maintenance. PNAS. 2009; 106:9304–9309. [PubMed: 19470484]
28. Eliazer S, Shalaby NA, Buszczak M. Loss of lysine-specific demethylase 1 nonautonomously causes stem cell tumors in the Drosophila ovary. PNAS. 2011; 108:7064–7069. [PubMed: 21482791]
29. Haynes SR, Raychaudhuri G, Beyer AL. The Drosophila Hrb98DE locus encodes four protein isoforms homologous to the A1 protein of mammalian heterogeneous nuclear ribonucleoprotein complexes. Mol Cell Biol. 1990; 10:316–323. [PubMed: 2104660]
30. Burd CG, Dreyfuss G. RNA binding specificity of hnRNP A1: significance of hnRNP A1 high-affinity binding sites in pre-mRNA splicing. EMBO J. 1994; 13:1197–1204. [PubMed: 7510636]
31. Misra S, et al. Annotation of the Drosophila melanogaster euchromatic genome: a systematic review. Genome Biol. 2002; 3:RESEARCH0083. [PubMed: 12537572]
32. Gilbert WV. Alternative ways to think about cellular internal ribosome entry. J Biol Chem. 2010; 285:29033–29038. [PubMed: 20576611]
33. Villa-Cuesta E, Sage BT, Tatar M. A Role for Drosophila dFoxO and dFoxO 53UTR Internal Ribosomal Entry Sites during Fasting. PLoS ONE. 2010; 5:e11521. [PubMed: 20634900]
34. Borah S, Wong AC, Steitz JA. Drosophila hnRNP A1 homologs Hrp36/Hrp38 enhance U2-type versus U12-type splicing to regulate alternative splicing of the prospero twintron. PNAS. 2009; 106:2577–2582. [PubMed: 19196985]
35. Bonnal S, et al. Heterogeneous nuclear ribonucleoprotein a1 is a novel internal ribosome entry site trans-acting factor that modulates alternative initiation of translation of the fibroblast growth factor 2 mRNA. Journal of Biological Chemistry. 2005; 280:4144–4153. [PubMed: 15525641]
36. Jo OD, Martin J, Bernath A, Masri J, Lichtenstein A, Gera J. Heterogeneous nuclear ribonucleoprotein A1 regulates cyclin D1 and c-myc Internal Ribosome Entry Site function through Akt signaling. Journal of Biological Chemistry. 2008; 283:23274–23287. [PubMed: 18562319]
37. Shi Y, Frost PJ, Hoang BQ, Benavides A, Sharma S, Gera JF, Lichtenstein AK. IL-6-induced stimulation of c-Myc translation in multiple myeloma cells is mediated by Myc internal ribosome entry site function and the RNA-binding protein, hnRNP A1. Cancer Research. 2008; 68:10215–10222. [PubMed: 19074889]
38. Lewis SM, Holcik M. For IRES trans-acting factors, it is all about location. Oncogene. 2007; 27:1033–1035. [PubMed: 17767196]
39. Leung AK, Vyas S, Rood JE, Bhutkar A, Sharp PA, Chang P. Poly(ADP-Ribose) Regulates Stress Responses and MicroRNA Activity in the Cytoplasm. Molecular Cell. 2011; 42:489–499. [PubMed: 21596313]
40. Oda H, Uemura T, Takeichi M. Phenotypic analysis of null mutants of *D*E-cadherin and Armadillo in *Drosophila* ovaries reveals distinct aspects of their functions in cell adhesion and cytoskeletal organization. Genes to Cells. 1997; 2:29–40. [PubMed: 9112438]

41. Fichelson P, Jagut M, Lepanse S, Lepesant JA, Huynh JR. Lethal giant larvae is required with the par genes for the early polarization of the Drosophila oocyte. Development. 2010; 137:815– 824. [PubMed: 20147382]

42. Hanai S, et al. Loss of poly(ADP-ribose) glycohydrolase causes progressive neurodegeneration in Drosophila melanogaster. PNAS. 2004; 101:82–86. [PubMed: 14676324]

43. Chou TB, Perrimon N. Use of a yeast site-specific recombinase to produce female germline chimeras in Drosophila. Genetics. 1992; 131:643–653. [PubMed: 1628809]

44. Duffy J, Harrison D, Perrimon N. Identifying loci required for follicular patterning using directed mosaics. Development. 1998; 125:2263–2271. [PubMed: 9584125]

45. Bakondi E, et al. Detection of poly(ADP-ribose) polymerase activation in oxidatively stressed cells and tissues using biotinylated NAD substrate. J Histochem Cytochem. 2002; 50:91398.

46. Walker J, Melo, Neto O, Standart N. Gel Retardation and UV-Crosslinking Assays to Detect Specific RNA-Protein Interactions in the 5′ or 3′ UTRs of Translationally Regulated mRNAs. Methods Mol Biol. 1998; 77:365–378. [PubMed: 9770682]

47. Goodrich JS, Clouse KN, Schüpbach T. Hrb27C, Sqd and Otu cooperatively regulate gurken RNA localization and mediate nurse cell chromosome dispersion in Drosophila oogenesis. Development. 2004; 131:1949–1958. [PubMed: 15056611]

48. Bolinger C, Yilmaz A, Hartman TR, Kovacic MB, Fernandez S, Ye J, Forget M, Green PL, Boris-Lawrie K. RNA helicase A interacts with divergent lymphotropic retroviruses and promotes translation of human T-cell leukemia virus type 1. Nucleic Acids Res. 2007; 35:2629–2642. [PubMed: 17426138]

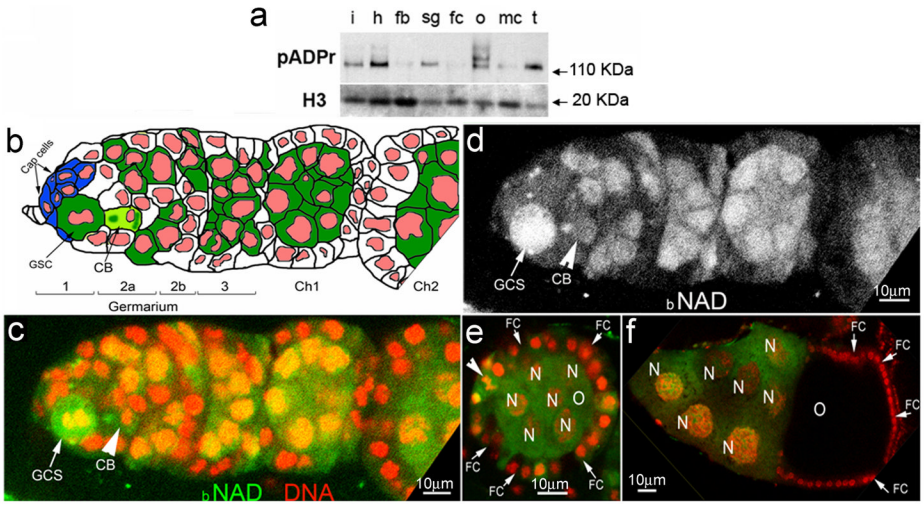

Figure 1. pADPr accumulates in mitotic germline stem cell and cystoblast

(**a)** The comparison of total cellular pADPr level in different tissues of *Drosophila* adult by Western blotting. The total protein from different tissues was immunoblotted with anti-pADPr antibody. The same blot was stripped and detected with anti-H3 antibody for loading control. i: intestines ; h: heads; fb: fat bodies; sg: salivary glands; fc: female carcasses; o: ovaries; mc: male carcasses; t: testes. (**b)** Schematic illustration of anterior part of *Drosophila* ovariole (matching **c** and **d** panels). Cap cells (blue) form germline stem cell (GSC) niche. CB: cystoblast; Ch1,Ch2: egg chambers 1 and 2. Germline cells are shown in green. Nuclei are shown in red. (**c–f)** Incorporation of the biotinylated NAD (bNAD) into *in vitro*-cultured *Drosophila* ovary. bNAD was detected using Avidin-Rhodamine staining (green). DNA was detected using oligreen dye (red). Strong accumulation of bNAD within dividing germline stem cell (GSC) (arrow), cystoblast (CB) (arrow) and in maturating germline cysts. **c.** Germarium and egg chamber 1. **d.** Germarium and egg chamber 1 (only bNAD is shown). (**e, f)** Egg chamber stages 4 (**e**) and 10 (**f**). O: oocyte; N: nurse cells; FC: follicle cells. Arrowhead indicates follicle cell in mitosis.

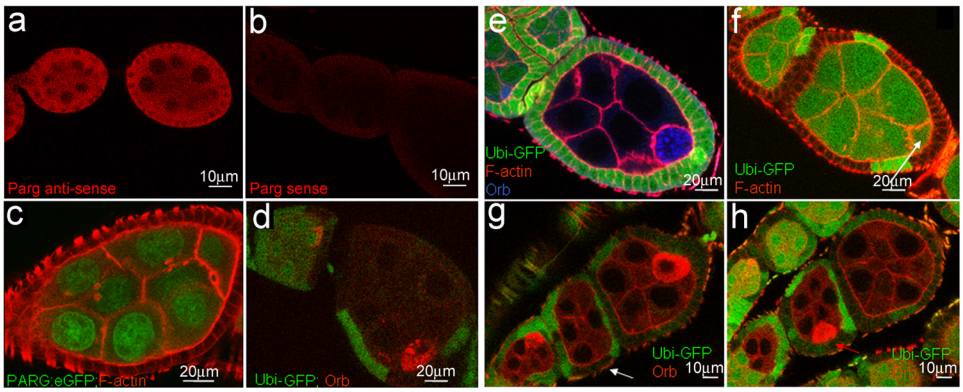

Figure 2. *Parg* expression in the ovary and mislocalization of the oocyte caused by *Parg* mutant clones

The anterior pole of all egg chambers is to the left, and the posterior pole is to the right. **(a)** *Parg* mRNA expression in the ovary of the wild type (*y,w*) detected by RNA *in situ* hybridization using *Parg* antisense probe. **(b)** The control of RNA *in situ* hybridization using *Parg* sense probe. **(c)** The expression of PARG-EGFP in the ovary induced by germline-specific GAL4 drivers. **(d)** The mock wild-type clones, including germline and polar follicle cells, showing the normal localization of the oocyte in the posterior. The oocyte is labeled with anti-orb antibody (red). The clones are generated from the female adults (FRT101/FRT101, ubi-GFP; FLP38/+) after heat shock. **(e)** *Parg* mutant germline clones showing the normal localization of the oocyte in the posterior. The germline clones are generated from the female adults ($Parg^{27.1}$, FRT101/FRT101, ubi-GFP; hs-FLP38/+) after heat shock. *Parg* mutant germline clones are shown by the absence of GFP expression (green); F-actin is stained with phalloidin to visualize the cell membrane, and the oocyte is labeled with anti-orb antibody (blue). **(f)** *Parg* mutant follicle cell clones showing the normal localization of the oocyte in the posterior. The follicle cell clones are generated from the female adults ($Parg^{27.1}$, FRT101/FRT101, ubi-GFP; en-Gal4,UAS-FLP38/+). *Parg* mutant follicle cell clones are shown by the absence of GFP expression (green). F-actin is stained with phalloidin to visualize the cell membrane. Arrow indicates the oocyte shown by the enrichment of F-actin in the ring canal. **(g)** *Parg* mutant germline and follicle cell clones in the anterior (white arrow). **(h)** *Parg* mutant clones, including germline and follicle cells, showing mislocalization of the oocyte in the lateral (red arrow). (**g,h**) *Parg* mutant germline and follicle cell clones are generated from the female adults ($Parg^{27.1}$,FRT101/FRT101,ubi-GFP; hs-FLP38/+) after heat shock and shown by the absence of GFP expression (green), and the oocyte is labeled with anti-orb antibody (red).

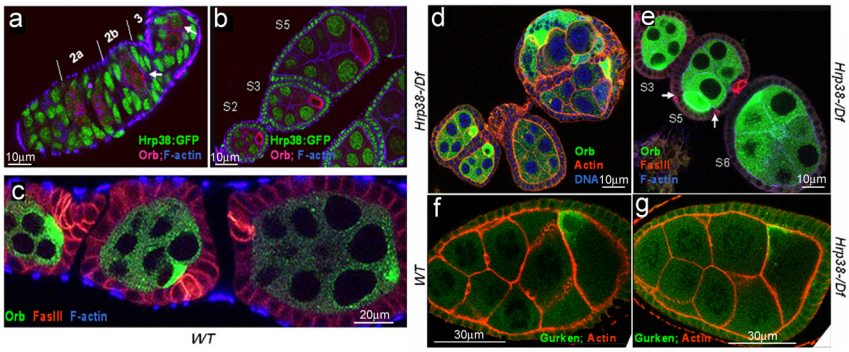

Figure 3. Ovary developmental defects caused by the*hrp38* mutations

(a–e) Egg chambers stained with phalloidin to visualize filamentous actin in the cell membrane and anti-orb antibody to label the oocyte. The anterior pole of all the egg chambers is to the left, and the posterior pole is to the right. **(a)** The Hrp38:GFP expression pattern in the germarium. Arrows indicate the pre-oocytes in region 2b and the oocyte in region 3. **(b)** The Hrp38:GFP expression pattern in the stage 2, 3 and 5 egg chambers. **(c)** The wild type in which the oocyte is localized in the posterior pole. The egg chambers were stained with anti-FasIII (red) for labeling the polar cells. **(d)** The *hrp38* hemizygotes showing the fused egg chambers. The egg chambers stained with Drag-5 (blue) to visualize DNA. **(e)** The *hrp38* hemizygotes showing mislocalization of the oocytes. Arrows indicate the separated polar cells stained with anti-FasIII (red) in the lateral where the oocyte is localized in the stage 5 egg chamber. **(f)** and **(g)** Gurken protein localization in the oocyte of the wild type **(f)** and the *hrp38* mutant **(g)**.

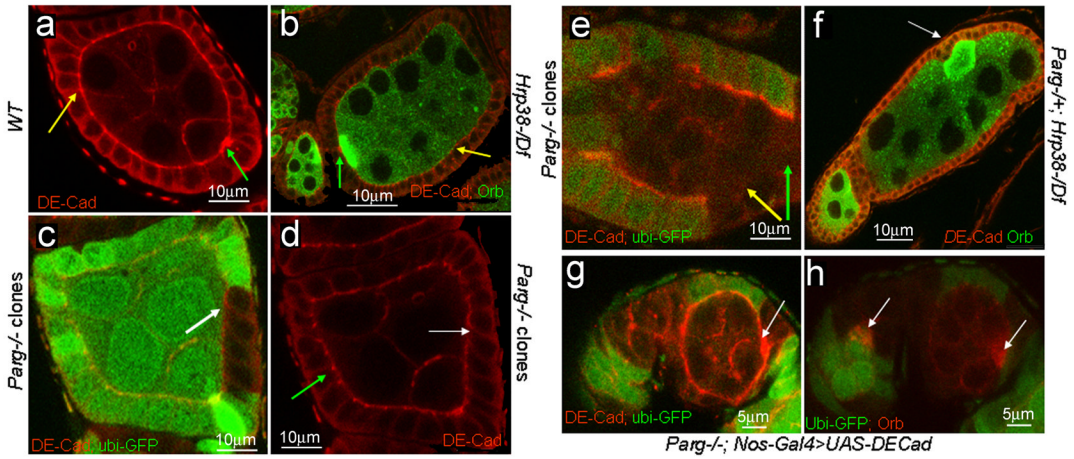

Figure 4. Regulation of DE-cadherin expression by pADPr modification of Hrp38

The anterior pole of all the egg chambers is to the left, and the posterior pole is to the right. **(a)** DE-cadherin expression in the egg chamber of the wild type. **(b)** DE-cadherin expression in the egg chambers of the *hrp38* mutant. The oocytes were labeled with anti-orb antibody. In **(a, b)**, green arrow indicates the interface between oocyte and anterior follicle cells (polar cells), and yellow arrow indicates the adherens junctions between the lateral follicle cells. **(c)** DE-cadherin expression in *Parg* follicle cell clones. *Parg* mutant follicle cell clones are shown by the absence of GFP expression. (**d**) DE-cadherin expression in the wild-type (green arrow) and *Parg* follicle cell clones (white arrow) as in (**c**). Arrows in (**c,d**) indicate the adherens junctions between the lateral follicle cells. **(e)** DE-cadherin expression in *Parg* germline and follicle cell clones. *Parg* mutant germline and follicle cell clones are shown by the absence of GFP expression (green). Green arrow indicates the interface between germline cells and posterior follicle cells, and yellow arrow indicates the adherens junctions between the lateral follicle cells. **(f)** DE-cadherin expression in the egg chambers of the genotype (*Parg*−/+; $hrp38^{d05172}/Df$). The oocyte (white arrow) is labeled with anti-orb antibody. **(g, h)** Expression of DE-cadherin in the germline rescued oocyte mislocalization in *Parg* mutant clones. The full genotype is (*Parg* $^{27.1}$, *FRT101/Ubi-GFP, FRT101; FLP38/ Nos-Gal4; UASp-DEcadherin/+*). **(g)** The elevated DE-cadherin expression (white arrow) in the posterior pole of one egg chamber with the *Parg* mutant germline and follicle cell clones, including the polar cells. **(h)** The normal oocyte localization (white arrow) in the same egg chamber as **(g).** The oocyte is labeled with anti-orb antibody (red).

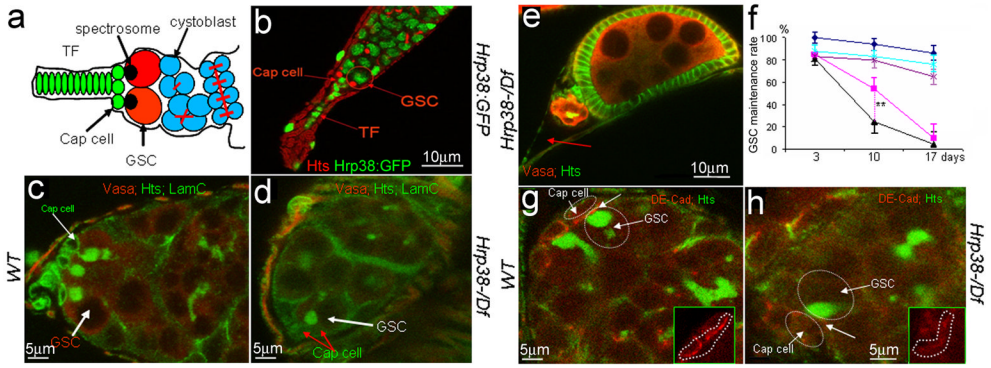

Figure 5. The *hrp38* gene is required for maintenance of germline stem cells (GSC)

(a) Simplified diagram of the germarium structure. GSCs having the round spectrosome are localized in the niche containing terminal filament (TF) and cap cells. The cystoblast and its progeny are interconnected through the ring canals. **(b)** The *hrp38* expression in GSC and cap cells in the tip of germarium of the Hrp38:GFP strain. GSC is labeled with anti-hts antibody for spectrosome (red). **(c)** 10-day-old germarial tip of the wild type. **(d)** 10-day-old germarial tip of the *hrp38* mutant. In **(c)** and **(d)**, GSCs are labeled with anti-hts (green) and anti-Vasa antibody (red). The cap cells are labeled with anti-Lam-C antibody (green). **(e)** 17-day-old germarium of the *hrp38* mutant showing the last egg chamber. The fusome in the last egg chamber is shown as yellow after labeling with anti-hts (green) and anti-Vasa antibody (red). Arrow indicates an empty germarium. **(f)** Graph showing GSC maintenance rate of the indicated genotypes. The GSC maintenance rate was based on the percent of the germaria with 2–3 GSCs at the indicated time after eclosion. Two germaria with one GSC was counted as one wild-type germarium to calculate their maintenance rate. **Symbols:** dark blue line with diamonds (the wild type) (n=85); pink line with squares (*hrp38*−/−) (n=82); black line with triangles (*Parg+/−; hrp38*−/−) (n=80); light blue with crosses (*RFP:Hrp38/ nos-Gal4; hrp38*−/−) (n=92); dark magenta line with stars (*DE-cad/nos-Gal4*; hrp38−/−) (n=110). The error bar represents the standard deviation of the proportion normalized with the sample size. ** P<0.01, analysed by *t*-test. (**g**) DE-cadherin expression in the 10-day-old GSC in the wild type. **(h)** DE-cadherin expression in the 10-day-old GSCs in the *hrp38* mutant. In **(g)** and **(h)**, GSCs are labeled with anti-hts (green). Inserts showed DE-cadherin expression in the interface (arrows) between GSC and the cap cells (circled).

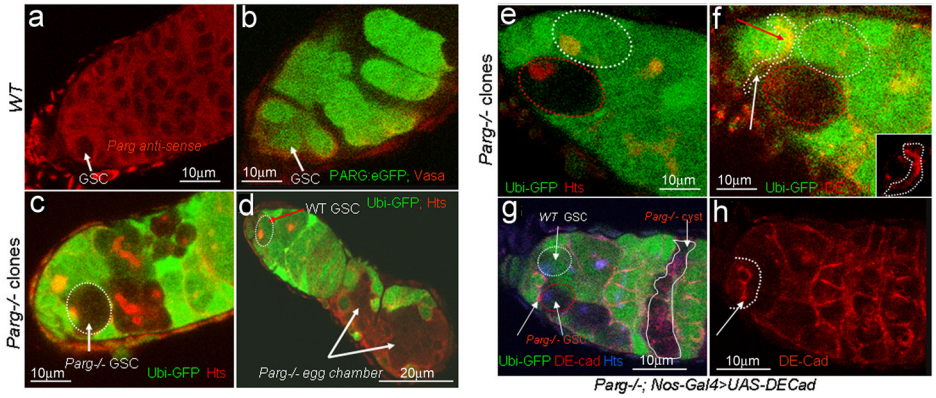

Figure 6. Loss of DE-cadherin expression in *Parg* mutant GSC

(a) *Parg* mRNA expression in GSC in the wild type (y,w), as detected by RNA *in situ* hybridization using *Parg* antisense probe. **(b)** The expression of PARG-EGFP in GSCs by germline-specific GAL4 drivers. **(c)** Germaria showing a 3-day-old *Parg* mutant GSC with loss of GFP expression. GSC is labeled with anti-hts (red). **(d)** 17-day-old germarium showing the loss of *Parg* mutant GSC. The loss of *Parg* mutant GSC was shown by the presence of two mutant egg chambers. GSC labeled with anti-hts antibody (red). **(e,f)** DE-cadherin expression in a germarium tip carrying one wild-type GSC and one *Parg* mutant GSC one week after clone induction. White cycle: the wild-type GSC (GFP positive); Red cycle: *Parg* mutant GSC (GFP-negative); GSCs are labeled with anti-hts antibody in **(e)**. Insert in **(f)** shows DE-cadherin expression in the interface between GSCs and wild-type cap cells (arrow indicated in **f**). **(g)** 17-day-old germarium showing *Parg* mutant GSC and its progeny. (**h**) Expression of DE-cadherin in the germline cells rescued *Parg* mutant GSC loss as shown in (**g**). The full genotype (**g** and **h**): *Parg* $^{27.1}$, *FRT101/Ubi-GFP, FRT101; FLP38/ Nos-Gal4; UASp-DEcadherin/+*. GSC labeled with anti-hts antibody (blue). Arrows in **(g and h)** indicate DE-cadherin expression in the interface between GSCs and wild-type cap cells.

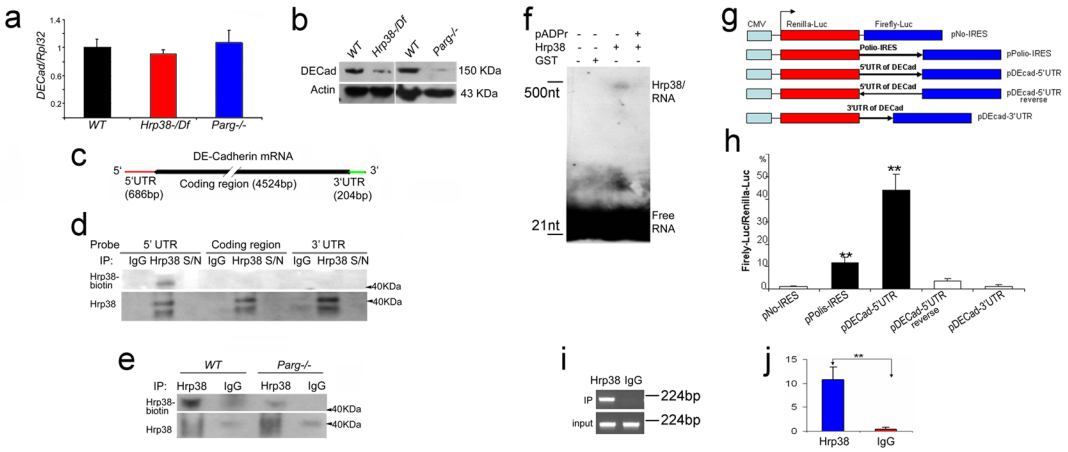

Figure 7. pADPr disrupts Hrp38 binding to 5′UTR of DE-cadherin conferring IRES activity

(a) The mRNA expression level of DE-cadherin in the different genotypes at the wandering third-instar larvae stage. **(b)** The protein expression level of DE-cadherin in the different genotypes at the wandering third-instar larvae stage. **(c)** The structure of DE-cadherin transcript. The biotin-labeled probes were made from three regions (5′UTR, coding region and 3′UTR). **(d)** Hrp38 binding to 5′UTR of DE-cadherin in the ovary is shown by UV-crosslinking analysis. The ovarian lysate from the wild-type fly (*y,w)* crosslinked to the biotin-labeled RNA probes as indicated was IPed with rabbit anti-Hrp38 antibody or normal rabbit IgG as the control for IP. The supernatant (S/N), which was obtained after each IP, was run in the same blot to show the efficiency of RNase treatment. **(e)** Decreased amounts of Hrp38 protein binding to 5′UTR of DE-cadherin in the *Parg* mutant. In **(d,e)** Hrp38 protein binding to biotin-labeled RNA probe was detected with Streptavidin. The same blot was stripped and probed with anti-Hrp38 antibody to show IP efficiency. **(f)** Inhibition of Hrp38 binding to its target RNA motif by poly(ADP-ribose). The biotin-labeled G-rich RNA element (**CAGGGCGCGCACUGUACGAG)** within 5′UTR of DE-cadherin was incubated with the components as indicated. **(g)** Diagrams of the different constructs for dual luciferase assay. pNO-IRES (negtative control); pPolio-IRES (positive control); pDEcad 5′UTR: *DE-cadherin* 5′UTR cloned into the vector in the forward orientation. pDEcad 5′UTR-reverse (spacer control); pDEcad-3′UTR (element control). **(h)** The ratio of firefly-to-renilla luciferase activity after the transfection of the different constructs as indicated into *Drosophila* S2 cells. **(i–j)** The association of Hrp38 with the transcript from pDEcad 5′UTR-luciferase construct shown by regular RT-PCR (**i**) and qRT-PCR (**j**) after RNA-IP. RNA IP was done using anti-Hrp38 antibody or rabbit IgG as a control after the transfection of pDEcad-5′UTR construct into S2 cells. The error bars in (h,j) represents the standard deviation from three independent experiments. $^{**}P \leq 0.01$, analyzed by *t*-test.

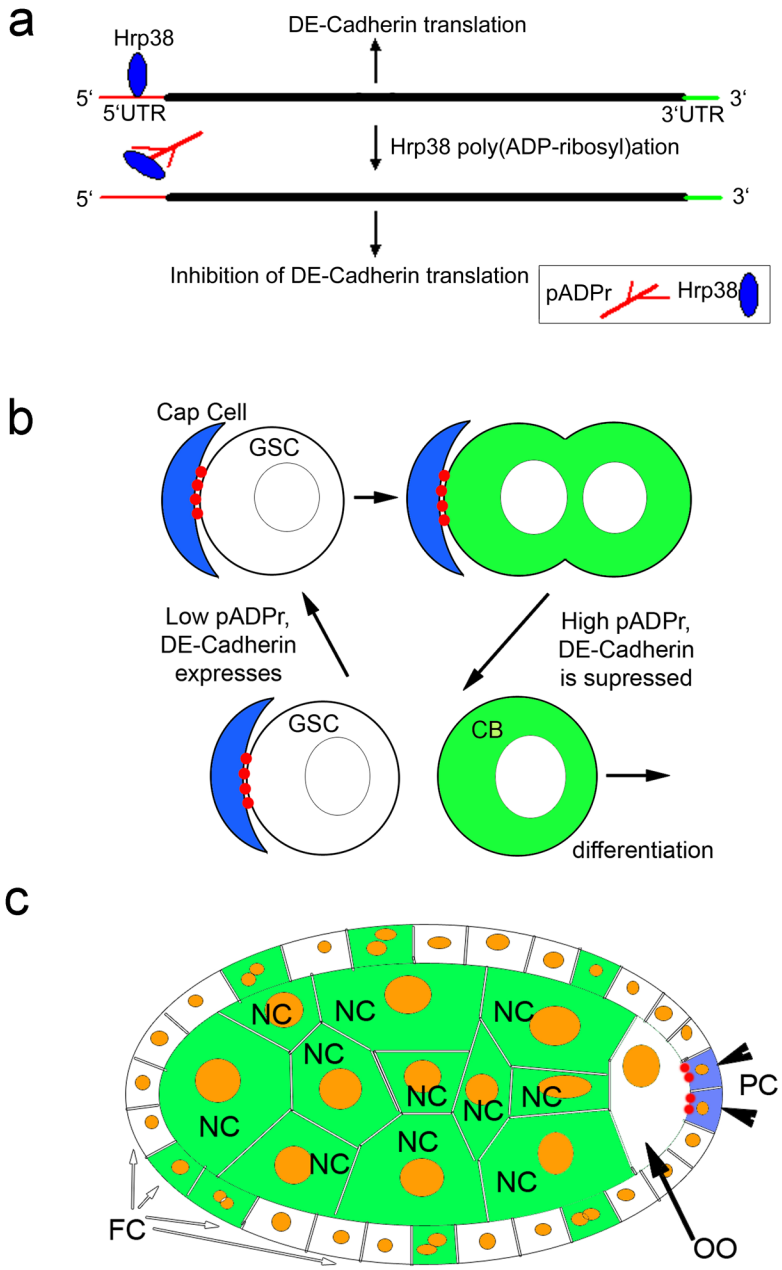

Figure 8. Diagram illustrating how Hrp38 modification by pADPr controls maintenance of GSC and oocyte localization

(a) pADPr binding to Hrp38 regulates DE-cadherin translation. Hrp38 binds to 5′UTR of DE-cadherin to promote translation by IRES-mediated manner. Once Hrp38 is modified with pADPr and dissociated from 5′UTR of DE-cadherin, its translation is inhibited. **(b)** pADPr modification of Hrp38 regulates DE-cadherin translation for germ-line stem cell (GSC) maintenance. DE-cadherin (red) accumulates in the interface between cap cells and GSC, keeping GSC in the stem cell niche. High level of pADPr (green) during mitosis and in cystoblasts suppresses translation of DE-cadherin. Suppression of DE-cadherin production promotes cystoblasts to leave stem cell niche and differentiate. **(c)** pADPr binding to Hrp38 regulates DE-cadherin translation for oocyte (OO) localization in maturating egg chamber. Low level of pADPr in the oocyte and mitotically quiescent polar

cells (PC) allows translating DE-cadherin (red) and positioning the oocyte in the posterior pole of the egg chamber. High level of pADPr (green) in nurse cells and mid-body follicle cells inhibits translation of DE-cadherin. FC - follicle cells.